

# Self-similar orbit-averaged Fokker-Planck equation for isotropic spherical dense clusters (ii) Physical properties and negative heat capacity of pre-collapse core

Yuta Ito<sup>a,b</sup>

<sup>a</sup>*Department of Physics, CUNY Graduate Center, <sup>☆</sup>*

<sup>b</sup>*Department of Engineering and Physics, CUNY College of Staten Island<sup>☆☆</sup>*

---

## Abstract

This is the second paper of a series of our works on the isotropic self-similar orbit-averaged Fokker-Planck (OAFP) equation and details physical properties of pre-collapse solution. The fundamental core collapse process at the late stage of relaxation evolution of spherical star clusters can be described by the self-similar OAFP equation. The accurate spectral solution was found recently in the first paper. The present work details the thermodynamical aspects of the model based on the stellar DF obtained from the solution. Our calculation shows the following local properties (i) Equation of state in the core is local ideal gas  $p = 1.0\rho/\chi_{\text{esc}}$  where the  $p$  is the pressure,  $\rho$  density and  $\chi_{\text{esc}}$  the scaled escape energy, while it is polytropic  $p = 0.5\rho^\Gamma/\chi_{\text{esc}}$  at large radii where  $\Gamma$  is the adiabatic index. (ii) If we consider the center is polytropic sphere, the polytropic index is 177. Also, as global property we construct caloric curves of the model to discuss the heat capacity together with Virial. Special focus is the cause of negative heat capacity of the core; the negativity is directly related to the deep potential well or large scaled escape energy through the criterion condition  $\phi = -6/\chi_{\text{esc}}$  where  $\phi$  is the central mean field potential in a well-relaxed core. Comparing our results to the previous works, we conclude, in the self-similar evolution, the negative heat capacity in the core holds due to collisionless and high-temperature stars that experience a rapid change in mean field potential through stellar- and heat- flow, rather than the isolation from surroundings due to self-gravity.

**Keywords:** dense star cluster; core collapse; self-similar evolution; orbit-averaged Fokker-Planck model; isotropic; negative specific heat; statistical mechanics

---

## 1. Introduction

This is the second paper of a series of our works on the isotropic self-similar orbit-averaged Fokker-Planck (ss-OAFP) equation. In the first paper (Ito, 2020), we found an accurate Gauss-Chebyshev spectral solution of the equation. The present work details the physical feature of the ss-OAFP model following the method established for equilibrium statistical mechanics of isotropic self-gravitating system. Section 1.1 explains the basic physical feature of the ss-OAFP model contrasting with basic isotropic self-gravitating models. Since the ss-OAFP model is essentially at a non-equilibrium state rather than equilibrium, Section 1.2 explains the assumptions we made. Especially, we focus on the negative heat capacity of the core of the ss-OAFP model. While the negative heat capacity of the equilibrium self-gravitating systems and systems of long- and short- range interacting particles have attracted one's concern, many of them focused only on equilibrium states (Section 1.3). We aim at showing the unique cause of the negative heat capacity of the core of the ss-OAFP model in the present paper.

### 1.1. Isotropic Self-gravitating system in equilibrium mechanics

One may list the isotropic models that could establish equilibrium statistical mechanics of self-gravitating (gaseous) systems based on what temperature one employs for the systems (Table 1)

---

<sup>☆</sup>365 Fifth Avenue, New York, NY 10016, USA

<sup>☆☆</sup>2800 Victory Boulevard, Staten Island, NY 10314, USA

Email address: yito@gradcenter.cuny.edu (Yuta Ito)

Model	Temperature	entropy	Ref
Isothermal sphere	Thermodynamic	Boltzmann	(Antonov, 1962; D. Lynden-Bell and Royal, 1968)
Energy-truncated models (e.g. <i>Woolly</i> , <i>King</i> and <i>Wilson</i> models)	Thermodynamic	Phenomenological	(Katz, 1980; Katz and Taff, 1983)
Stellar Polytrope	Polytropic (constant)	Tsallis's	(Taruya and Sakagami, 2002; Chavanis, 2002b)
ss-OAFP models	?	?	

Table 1: Typical isotropic self-gravitating systems discussed for study on equilibrium statistical mechanics.

The ss-OAFP model would have three different (non-)equilibrium states. In the core the stars could behave like an isothermal sphere due to frequent two-body relaxation events. The inner halo would be a receiver of heat- and stellar (particle-) fluxes due to the escaping stars from the core, resulting in a non-equilibrium state. In the outer halo, self-similar analysis<sup>1</sup> extends the inner halo to infinite radius (without or with very little stellar and energy- fluxes) and the outer halo would behave like a collisionless system forming a power-law profile at a state of Tsallis equilibrium (Refer to Tsallis, 2009, for detail of Tsallis's generalized statistical dynamics).

### 1.2. Assumptions made for the ss-OAFP model

To discuss thermodynamical aspects of the ss-OAFP model, one needs several assumptions. For example, the system can reasonably exist only in a time-averaged sense due to the discreteness (finiteness of total number of stars) of star clusters. Hence, to consider the system a thermodynamic system, it must be an 'exotic' self-gravitating gas at a stationary non-equilibrium state, composed of  $N(>> 10^6 >> 1)$  particles whose distribution function (DF) and mean field (m.f.) potential follow the solution of the ss-OAFP model at a certain time of self-similar evolution. The meaning of 'exotic' is here that the gas has intrinsically *negative* heat capacity as its normal state (at least in the core of the system) as explained in the following sections. In addition, the ss-OAFP model is not isolated, which implies the model can not reach a QSS in the sense that Virial ratio can not reach unity. Hence one may expect the model may not achieve an equilibrium state but still can be at stationary in the inner- and outer- halos (in case of self-similar model). For the rest, following the classical discussion (Antonov, 1962; D. Lynden-Bell and Royal, 1968), we consider the ss-OAFP model is enclosed by an adiabatic spherical wall of radius  $R(\Phi)$ , where  $\Phi$  is the m.f. potential  $\phi(r, t)$  in self-similar form, that elastically reflects star on the inner surface. The present work employs the reference solution  $F_o(E)$  and  $\Phi_o(R)$  as stellar DF and m.f. potential obtained in (Ito, 2020) for further discussion.  $F_o(E)$  and  $E$  are the self-similar forms of probability density DF  $f(\epsilon, t)$  and energy  $\epsilon$  that is available to star at phase point  $(\mathbf{r}, \mathbf{v})$  orbiting in an isotropic star cluster at time  $t$ . Also, we assume the time  $t$  of the ss-OAFP model is fixed to a certain time  $t_c$ . This means the time-dependent variables (e.g.  $f_t, g_t, \epsilon_t, \dots$ ) in (Ito, 2020) turn into the factors that make the self-similar variables (e.g.  $F, G, R, \dots$ ) in dimensionless form.

### 1.3. The cause of negative heat capacity reported in the previous works

Negative heat capacity has been discussed not only for self-gravitating astrophysical objects such as stars, star clusters and black holes (Lynden-Bell, 1999) but also stratified gasses (Ingel, 2000), proteins (Prabhu and Sharp, 2006), granular gasses (Brilliantov et al., 2018) and systems of small  $N$  particles such as Lennard-Jones gas (Thirring et al., 2003), melting metal clusters (Aguado and Jarrold, 2011) and hot nuclei (Borderie and Frankland, 2019). Many of existing works are based on numerical simulations and analytical approaches though, the negative heat capacity itself is not just a theoretical outcome. Laboratory experiments have shown the signature of negative specific capacity of nuclear fragmentation (DéAgostino et al., 1999, 2000; Srivastava, 2001; Gobet et al., 2002) and of melting metal

<sup>1</sup>More realistic arguments for finite outer halo needs to include the effect of flux at the ridge of cluster, two dimensional (anisotropic) effect, and escapers and escaping stars with high eccentricity under the influence of tidal effects. The discussions for the outer halo are found in (e.g. Michie, 1962; Spitzer and Shapiro, 1972; Claydon et al., 2019).

clusters (Schmidt et al., 2001). The existing works commonly focus on microcanonical ensembles and yield that the negative heat capacity occurs in an energy band on which the system undergoes a phase transition such as 'gas'- 'liquid' and 'liquid'- 'solid'. In case of the star cluster the transition corresponding to 'gas'- 'collapsed-state' in which 'gas' corresponds with a state of self-gravitating gas with positive heat capacity and 'collapsed-state' means a state of core-halo structure with negative heat capacity. For brevity, our interest is negative heat capacity of the core of the ss-OAFP model and it is considered a system of small numbers ( $N \ll 10^5$ ) of stars.

For discussion of negative heat capacity, one typically concerns with inhomogeneous microcanonical ensemble, which may be explained by discussing the systems that do *not* undergo negative heat capacity. In case of an thermodynamic-equilibrium small  $N$  system of homogeneous subsystems e.g. nanoclusters. (Michaelian and Santamaría-Holek, 2007; Lynden-Bell and Lynden-Bell, 2008; Michaelian and Santamaría-Holek, 2015, 2017), negative heat capacity does not occur regardless of kind of statistical ensembles. Commonly the negative heat capacity has been reported for microcanonical ensemble (Lynden-Bell, 1999) though, the small  $N$  systems can not achieve ergodicity due to particles being generally trapped only in limited part of the whole phase space, meaning less mixing process occurs in the system and the final state (and heat capacity) should depend on the initial condition. On one hand, in case of inhomogeneous equilibrium systems, negative heat capacity does not occur for canonical ensemble (Thirring, 1970; Lynden-Bell and Lynden-Bell, 1977) and grandcanonical ensemble (Josephson, 1967) since the heat capacities are defined by the square of fluctuation in thermodynamic quantities in the same way as the homogeneous case. These discussions typically suggests negative heat capacity could occur only for (isolated) inhomogeneous system in microcanonical ensemble (Lynden-Bell and Lynden-Bell, 2008).

Although the negative heat capacity has been found in (nearly) isolated astrophysical systems of particles or stars interacting via Newtonian potential, the long-range nature of pair-wise potential itself is not only the cause of the negativeness. For example, even non-interacting particles can have negative heat capacity under certain background potentials. Based on Virial theorem and toy models, Einarsson (2004) showed collisionless particles in the background potential profile  $\sim r^a$  (in three dimension) provides negative heat capacity if  $a = -1$  while if  $a \neq -1$  it does not. Thirring et al. (2003); Carignano and Gladich (2010) showed negative heat capacity can occur to collisionless particles under a sudden change in a potential change from a deep narrow potential well at small radii toward a shallow wide well at larger radii. On one hand, even without a background potential well, particles interacting through short-range pair potential can reveal negative heat capacity. The examples are Lennard-Jones potential for small  $N$  ( $\sim 10$ ) (Thirring et al., 2003) and Gaussian potential (Posch et al., 1990; Posch and Thirring, 2005) for  $N \sim 100$ .

We aim at finding the cause of negative specific heat in the core of the ss-OAFP model after detailing the physical feature of the model based on the moments of the reference DF and Virial. The present paper is organized as follows. Section 2 shows the local and global properties of the ss-OAFP model based on the moments of the reference DF. Section 3 aims to construct an analogue of caloric curve and show negative heat capacity at constant volume for the model after regularizing the thermodynamic quantities. Section 4 explains the cause of the negative heat capacity in the core of the ss-OAFP model by comparing the core to existing models. Section 5 is Conclusion.

## 2. Thermodynamic quantities of the ss-OAFP model

Since the previous works (Heggie and Stevenson, 1988; Takahashi, 1993) did not discuss the detail structure of the ss-OAFP model unlike (Lynden-Bell and Eggleton, 1980)'s work for a self-similar conductive gaseous model, we extend (Lynden-Bell and Eggleton, 1980)'s analyses to the ss-OAFP model, especially focusing on the core. Sections 2.1 and 2.2 detail the local- and global- properties of the ss-OAFP model.

### 2.1. Local properties of the ss-OAFP model

The stellar DF of the ss-OAFP model may not be even a local Maxwellian DF, hence we need to find the moments of the DF (i.e. local thermodynamic- or hydrodynamic- quantities) to capture the physical features of the model. In addition to density  $\rho(r, t)$  and its self-similar form  $D(\Phi)$  (calculated for the ss-OAFP equation in (Ito, 2020),

one may define the velocity dispersion, pressure and heat- and stellar- fluxes in terms of moments of DF

$$v^2(r, t_c) = \frac{1}{\rho(r, t_c)} \int_{\phi(r, t_c)}^0 (2\epsilon - 2\phi(r, t_c))^{3/2} f(\epsilon, t_c) d\epsilon, \quad (2.1a)$$

$$p(r, t_c) = \frac{v^2(r, t_c) \rho(r, t_c)}{3}, \quad (2.1b)$$

$$f^h(r, t_c) = -k \frac{\partial v^2(r, t_c)}{\partial r}, \quad (2.1c)$$

$$f^p(r, t_c) = -\mathcal{D} \frac{\partial \rho(r, t_c)}{\partial r}, \quad (2.1d)$$

where  $k$  is the thermal conductivity and  $\mathcal{D}$  the diffusivity. Since the value of  $k$  (and  $\mathcal{D}$ ) depends on the definition of relaxation time concerned (Lynden-Bell and Eggleton, 1980; Louis and Spurzem, 1991) we regularize the heat- and stellar- fluxes by the constants in the coefficients in self-similar analysis (by  $3GmC_k \ln[N]$  for the conductivity and  $\sqrt{2C_D \ln[N]}/3$  for the diffusivity<sup>2</sup>, where  $m$  is stellar mass,  $G$  is the gravitational constant and  $C_k$  and  $C_D$  are dimensionless constants of approximately unity.). Employing the self-similar variables in (Ito, 2020) and introducing new dimensionless variables

$$v^2(r, t_c) = V_{(\text{dis})}^2(R) v_t^2(t) \equiv 2V_{(\text{dis})}^2(R) \epsilon_t(t), \quad (2.3a)$$

$$p(r, t_c) = P(R) p_t(t), \quad (2.3b)$$

$$\frac{f^h(r, t_c)}{3GmC_k \ln[N]} \equiv \mathcal{F}^h(R) f_t^h(t_c), \quad (2.3c)$$

$$\frac{f^p(r, t_c)}{2C_D \ln[N]/3} \equiv \mathcal{F}^p(R) f_t^p(t_c), \quad (2.3d)$$

where  $S(\Phi) = -2S(x)$  due to the definition in (Ito, 2020), the local quantities in dimensionless form read

$$V_{(\text{dis})}^2(R) = 2 \frac{U_{3/2}(\Phi)}{U_{1/2}(\Phi)}, \quad (2.4a)$$

$$P(R) = \frac{2}{3} U_{3/2}(\Phi), \quad (2.4b)$$

$$\mathcal{F}^h(R) = -\frac{U_{1/2}(\Phi)}{S(\Phi) \sqrt{V_{(\text{dis})}^2(\Phi)}} \left( \frac{U_{3/2}(\Phi) U_{-1/2}(\Phi)}{[U_{1/2}(\Phi)]^2} - 3 \right), \quad (2.4c)$$

$$\mathcal{F}^p(R) = -\frac{1}{\sqrt{V_{(\text{dis})}^2(\Phi)}} \frac{U_{-1/2}(\Phi)}{S(\Phi)}, \quad (2.4d)$$

where  $U_n(\Phi)$  is

$$U_n(\Phi) = \int_{\Phi}^0 F(E) (E - \Phi)^n dE. \quad (2.5)$$

where  $n$  is a real number; for example, if  $n = 1/2$  then  $U_n(\Phi) = D(\Phi)$ .

The ss-OAFP model has characteristics similar to those of the self-similar conductive gaseous model reported in (Lynden-Bell and Eggleton, 1980). Figure 1(a) depicts the velocity dispersion  $V_{(\text{dis})}^2$  and m.f. potential profile  $\Phi$ . The

<sup>2</sup>For the conductivity the expression followed (Lynden-Bell and Eggleton, 1980). In a similar way, the diffusivity is calculated as follows

$$\mathcal{D} = \frac{1}{3} l \sqrt{v^2} \approx \frac{1}{3} \frac{C_D}{k_j^2 T_R} = \frac{1}{3} \frac{v^2(r, t_c)}{4\pi G \rho(\phi(r, t_c))} \frac{8\pi G m C_D \rho(\phi, t_c) \ln[N]}{[v^2(r, t_c)]^{3/2}} = \frac{2C_D \ln[N]}{3 \sqrt{v^2(r, t_c)}}. \quad (2.2)$$

where  $l$  is the mean free path of stars,  $k_j$  is the inverse of Jeans length and  $T_R$  is the relaxation time from (Spitzer, 1988).

constancy of  $V_{\text{(dis)}}^2$  further extends in radius compared to that of  $\Phi$ . Figure 1(b) shows the heat flux  $\mathcal{F}^h$  and stellar flux  $\mathcal{F}^p$ .  $\mathcal{F}^h$  reaches its maximum at  $R = 4.31$ . This radius is relatively close to  $R = 8.99$  at which the gravothermal instability occurs for the isothermal sphere in canonical ensemble (D. Lynden-Bell and Royal, 1968).  $\mathcal{F}^p$  reaches its maximum at slightly smaller radius,  $R = 3.11$ . As the local relaxation time increases with radius,  $\mathcal{F}^h$  and  $\mathcal{F}^p$  rapidly decreases while  $\mathcal{F}^p$  decays slightly slowly compared to  $\mathcal{F}^h$ . The location of the maximum stellar flux can be explained by the escape speed of stars yet, which is discussed in Section 2.2 (since the speed is a global property of the cluster.) The tuning points for fluxes seem slightly different from the graphed maximum value in (Lynden-Bell and Eggleton, 1980) but the qualitative nature of our velocity dispersion, m.f. potential and fluxes little differ from the gaseous models.

The present work further details the self-similar model based on adiabatic index and local state of equation that have not been discussed in detail for self-similar models. Following (Cohn, 1980)'s analyses on time-dependent OAFP model, we calculated the polytropic index  $m \equiv \beta + 3/2$  of ss-OAFP model. Figure 2 depicts the adiabatic index  $\Gamma (\equiv 1 + 1/m)$  and polytropic index  $m$  against dimensionless radius  $R$ . We calculated  $\Gamma$  taking the logarithmic derivative  $d \ln[P(R)] / d \ln[D(R)]$ . The result shows a distinctive nature in the structures of the core, inner-halo and outer-halo. In the outer halo,  $m$  asymptotically reaches 9.67837115... ( $\Gamma \approx 1.10$ ) for large  $R$ .<sup>3</sup> For small  $R$  or in the core and inner halo, one can find two two features. (i)  $m$  reaches its minimum value 8.52 ( $\Gamma = 1.117$ ) at  $R = 157$ ; (ii)  $m$  increases with decreasing  $R$  and reaches 177 ( $\Gamma = 1.00564$ ) at the center of the core. Higher  $m$  (or  $\Gamma$  close to unity) implies the core behaves like an isothermal sphere. Given  $\Gamma$ , one can find the asymptotic form for the equation of local state (Figure 3). As expected, the core is approximately an ideal gas with the thermodynamic temperature  $1/\chi_{\text{esc}}$  while the outer halo follows a polytrope of  $m = \beta_o + 3/2$  and has a temperature approximately half of  $1/\chi_{\text{esc}}$  if the polytropic constant  $K$  (in  $p(r, t_c) = K\rho(r, t_c)^\Gamma$ ) is considered the constant temperature of the polytrope;

$$P = \frac{1.0}{\chi_{\text{esc}}} D, \quad (R \approx 0) \quad (2.6a)$$

$$P = \frac{0.5}{\chi_{\text{esc}}} D^\Gamma. \quad (R \rightarrow \infty) \quad (2.6b)$$

where the inverse temperature of the ss-OAFP model is  $\chi_{\text{esc}}$ .

## 2.2. Global properties of the ss-OAFP model

Global properties of the ss-OAFP model can provide understanding of the macroscopic structure as comparison to local properties (Section 2.1). Yet, it is hard to conceptualize some thermodynamic quantities for non-equilibrium state, hence the present work avoids exactly defining entropy and the thermodynamic zeroth law. The total- mass, kinetic energy and potential energy of stars that are confined by an adiabatic wall at radius  $R_M$  read

$$M(R_M, t_c) = \iint m f(\epsilon, t_c) d^3v d^3r, \quad (2.7a)$$

$$\text{KE}(R_M, t_c) = \iint m \frac{v^2}{2} f(\epsilon, t_c) d^3v d^3r, \quad (2.7b)$$

$$\text{PE}(R_M, t_c) = \iint m \phi(r, t_c) f(\epsilon, t_c) d^3v d^3r, \quad (2.7c)$$

$$E_{\text{tot}}(R_M, t_c) = \text{KE} + \text{PE}. \quad (2.7d)$$

<sup>3</sup>The value of  $m$  holds the relative error  $6.3 \times 10^{-10}\%$  from the expected value  $\beta_o + 3/2$ .

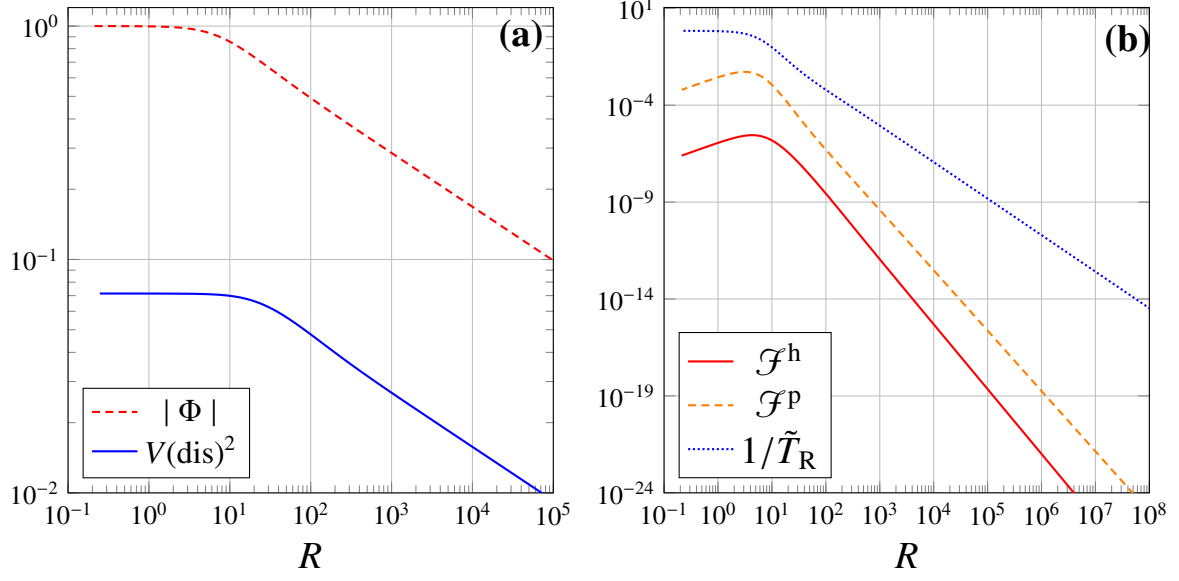


Figure 1: **(a)** Dimensionless m.f. potential  $\Phi$  and velocity dispersion  $V(\text{dis})^2$  and **(b)** dimensionless heat flux  $\mathcal{F}^h$  and stellar flux  $\mathcal{F}^p$ . The latter also depicts the inverse of regularized local relaxation time  $\tilde{T}_R (= D(\phi, t_c)/[v^2(r, t_c)]^{3/2})$  for comparison.

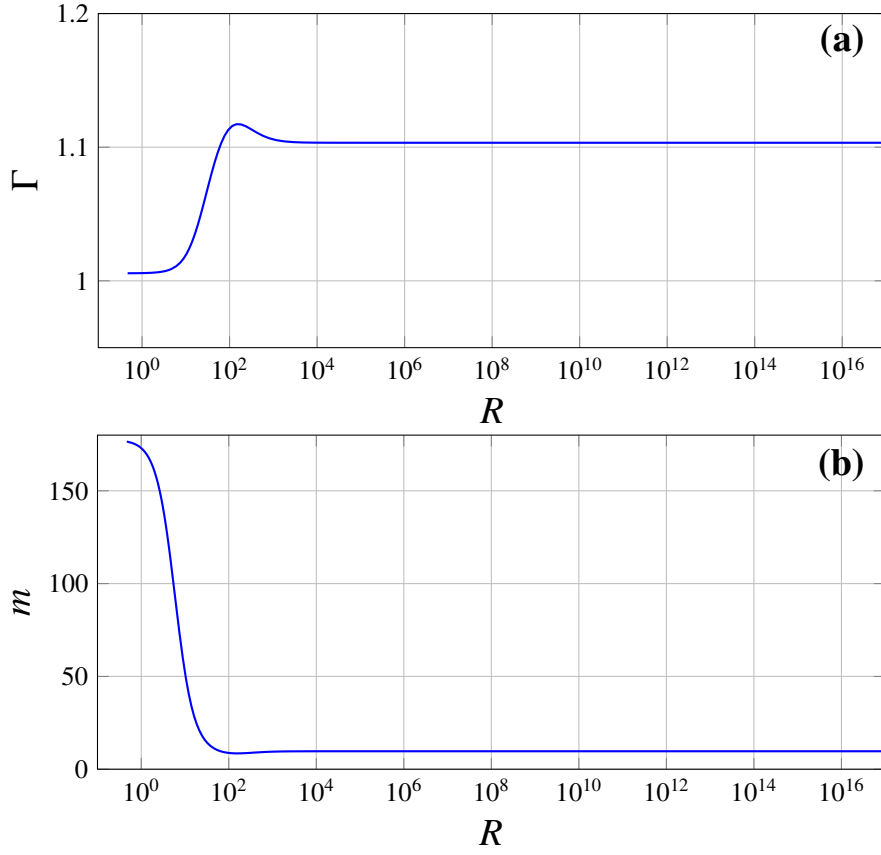


Figure 2: **(a)** Adiabatic index  $\Gamma$  and **(b)** polytropic index  $m$  of the ss-OAFP model.

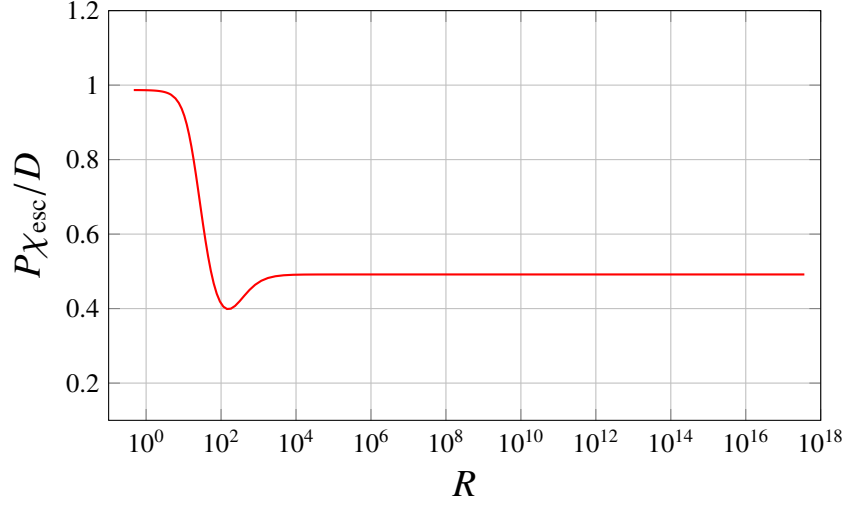


Figure 3: Local equation of state with constant thermodynamic temperature  $\chi_{\text{esc}}$ .

The dimensionless forms are

$$M(\Phi_M) \equiv \frac{M(r, t_c)}{M_t(t_c)} = - \int_{-1}^{\Phi_M} DR^2 S \, d\Phi, \quad (2.8a)$$

$$\text{KE}(\Phi_M) \equiv \frac{\text{KE}(r, t_c)}{\text{PE}_t(t_c)} = - \int_{-1}^{\Phi_M} U_{3/2} R^2 S \, d\Phi, \quad (2.8b)$$

$$\text{PE}(\Phi_M) \equiv \frac{\text{PE}(r, t_c)}{\text{PE}_t(t_c)} = \frac{1}{2} \int_{-1}^{\Phi_M} \Phi DR^2 S \, d\Phi, \quad (2.8c)$$

$$E_{\text{tot}}(\Phi_M) \equiv \frac{E_{\text{tot}}(r, t_c)}{\text{PE}_t(t_c)}, \quad (2.8d)$$

where  $\Phi_M$  is the potential at the wall radius  $R_M$  and the corresponding variables at time  $T_c$  have the following relation

$$M_t(t_c) = (4\pi)^2 \sqrt{2} m f_t(t_c) [E_t(t_c)]^{3/2} [r_t(t_c)]^3, \quad (2.9a)$$

$$\text{PE}_t(t_c) = \frac{\text{KE}_t(t_c)}{2} = \frac{1}{2} M_t(t) E_t(t_c). \quad (2.9b)$$

Since the thermodynamic temperature  $\chi_{\text{esc}}$  can not be defined properly as a global quantity for the ss-OAFP model, one may heuristically introduce the kinetic temperature  $T^{(\text{kin})}$  and local temperature  $T^{(\text{loc})}$

$$T^{(\text{kin})}(\Phi_M) \equiv \frac{2\text{PE}}{3M}, \quad (2.10a)$$

$$T^{(\text{loc})}(R_M) \equiv \frac{V_{(\text{dis})}^2}{3}. \quad (2.10b)$$

Figure 4 depicts the local- and kinetic- temperatures. At the center of the system the temperatures hold approximately a constant profile.<sup>4</sup> Hence, if focusing on the behavior in the core, one may approximately define the inverse temperature of Maxwellian DF in standard context of statistical mechanics<sup>5</sup> as follows

$$\beta^{(\text{con})} \equiv \frac{\chi_{\text{esc}}}{\epsilon_t(t_c)}, \quad (2.11)$$

<sup>4</sup>Of course exactly speaking, the temperatures gradually decreases with radius and the maximum temperatures are lowered by 1 % approximately at  $R \approx 2.1$  for local temperature and  $R \approx 2.7$  for kinetic one.

<sup>5</sup>We still do not discuss the relation of the temperature with entropy even if the system is considered an isolated system.

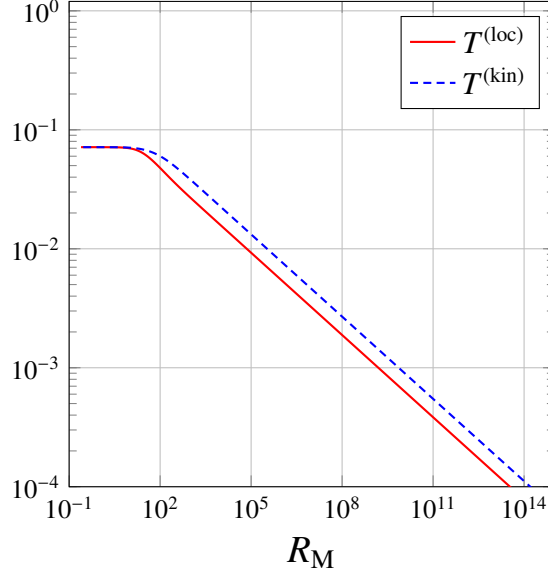


Figure 4: Local temperature and kinetic temperature.

This provides an approximate relationship at the center of the system

$$T^{(\text{loc})} R_M r_t(t_c) \approx T^{(\text{kin})} R_M r_t(t_c) \approx \frac{1}{k_B \beta^{(\text{con})}}, \quad (2.12a)$$

$$T^{(\text{loc})}(\Phi_M) \approx T^{(\text{kin})}(\Phi_M) \approx \chi_{\text{esc}}, \quad (2.12b)$$

where  $k_B$  is the Boltzmann constant.

One also can calculate the escape speed from the cluster to explain the maximum and rapid decay of the stellar flux  $\mathcal{F}^P$  in Figure 1. First, we introduce the following escape speeds in dimensionless form

$$v_{\text{esc}}^{(\text{PE})} = \sqrt{-4\text{PE}}, \quad (2.13a)$$

$$v_{\text{esc}}^{(\text{con})} = \sqrt{4 \frac{M}{R_M}}, \quad (2.13b)$$

where  $v_{\text{esc}}^{(\text{con})}$  is introduced based on Virial theorem considering the core is the isothermal sphere isolated from the halo. Figure 5 compares the escape speeds to stellar flux  $\mathcal{F}^P$ . In the core, velocity dispersion  $\sqrt{V_{(\text{dis})}^2}$  is greater than the escape speeds. Yet, at the center of the core there is less mass flux due to the flattening. On one hand, as  $R_M$  increases, decreasing density (or the transition to inner halo from the core) causes the increasing stellar flux. Beyond  $R = 2.2 \sim 2.3$  at which  $\sqrt{V_{(\text{dis})}^2}$  is order of the escape speeds, stars can hardly escape due to the self-gravity of the cluster hence stellar flux decays rapidly with  $R_M$ .

### 3. Regularized thermodynamic quantities and negative heat capacity

The present section focuses on the core of the ss-OAFP model to discuss the negative heat capacity. Section 3.1 regularizes the total energy and temperatures and Section 3.2 depicts the caloric curve to characterize the negative heat capacity.



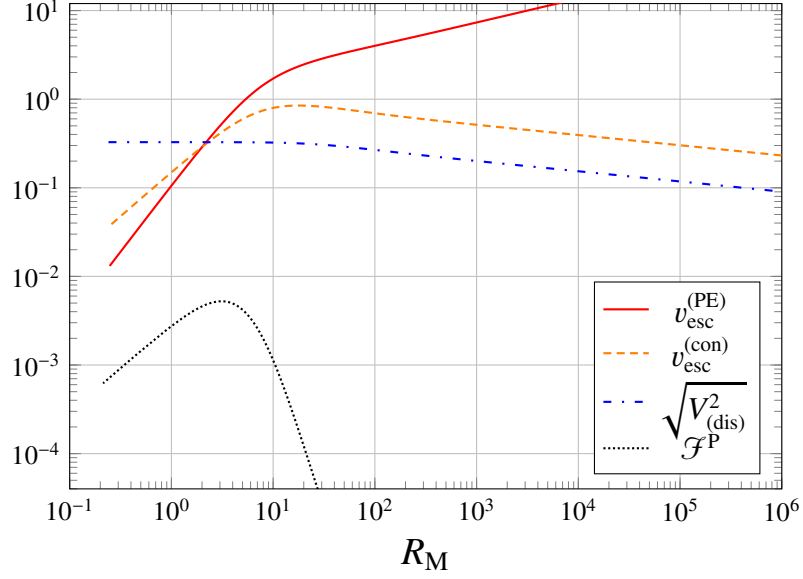


Figure 5: Escape speeds of stars. As comparison, the stellar flux  $\mathcal{F}^P$  and velocity dispersion  $\sqrt{V_{(\text{dis})}^2}$  are depicted.

### 3.1. Regularized thermodynamic quantities

One would like to consider even for inhomogeneous thermodynamic systems of log-range interacting stars that there exists a thermodynamic limit in the same way as the standard limit  $N/V \rightarrow \text{const.}$  if  $N \rightarrow \infty$  and  $V \rightarrow \infty$  for homogeneous systems of particles undergoing short-range interaction. Also, since the mass, energy and size of the ss-OAFP model are infinite, one needs a proper thermodynamic limit to regularize thermodynamic quantities with the wall  $R_M$ . For total energy, the following normalization has been employed for the isothermal sphere (Antonov, 1962; D. Lynden-Bell and Royal, 1968) based on Boltzmann entropy and polytropes (Taruya and Sakagami, 2002; Chavanis, 2002b) based on Tsallis entropy

$$\Lambda = \frac{rE_{\text{tot}}(r, t_c)}{GM^2(r, t_c)} = \frac{R_M E_{\text{tot}}(\Phi_M)}{[M(\Phi_M)]^2}. \quad (3.1)$$

This regularization originates from the feature of Poisson equation (Appendix A). Figure 6 shows the regularized total energy  $\Lambda$  of the ss-OAFP model, compared to that of the isothermal sphere. The energy of the ss-OAFP model is negative at all radii, meaning that the system is dominated by the potential energy. Statistical dynamicists term this state (or turning point) a 'collapsed phase' that occurs to the isothermal sphere (and polytropes of  $m > 5$ ) enclosed by an adiabatic wall of a large radius. The energy  $\lambda$  reaches order of unity under the following relation with the limit  $N \rightarrow \infty$  (sometimes the relation and limit are called the *dilute* limit (e.g. de Vega and Sánchez, 2002; Destri and de Vega, 2007) that corresponds to one of Boltzmann-Knudsen limits in standard gaseous kinetic theory)

$$R_M \propto N, \quad (3.2a)$$

$$M(\Phi_M) \propto N, \quad (3.2b)$$

$$E_{\text{tot}}(\Phi_M) \sim \text{KE}(\Phi_M) \sim \text{PE}(\Phi_M) \propto N, \quad (3.2c)$$

$$1/\beta^{(\text{con})} \propto 1, \quad (3.2d)$$

This limit determines only the relations among the magnitudes of quantities. The important point is that there exists some reasonable dimensionless parameter as  $R_M \rightarrow \infty$ .<sup>6</sup> In a similar way, one can convert the reciprocal of the

<sup>6</sup>For example, density (cluster) expansion in thermodynamic limit does not mean a density  $n$  itself is the expansion parameter, rather the corresponding (dimensionless) occupation number  $\frac{4}{3}na^3$ , where  $a$  is the characteristic size of particles, is the actual parameter.

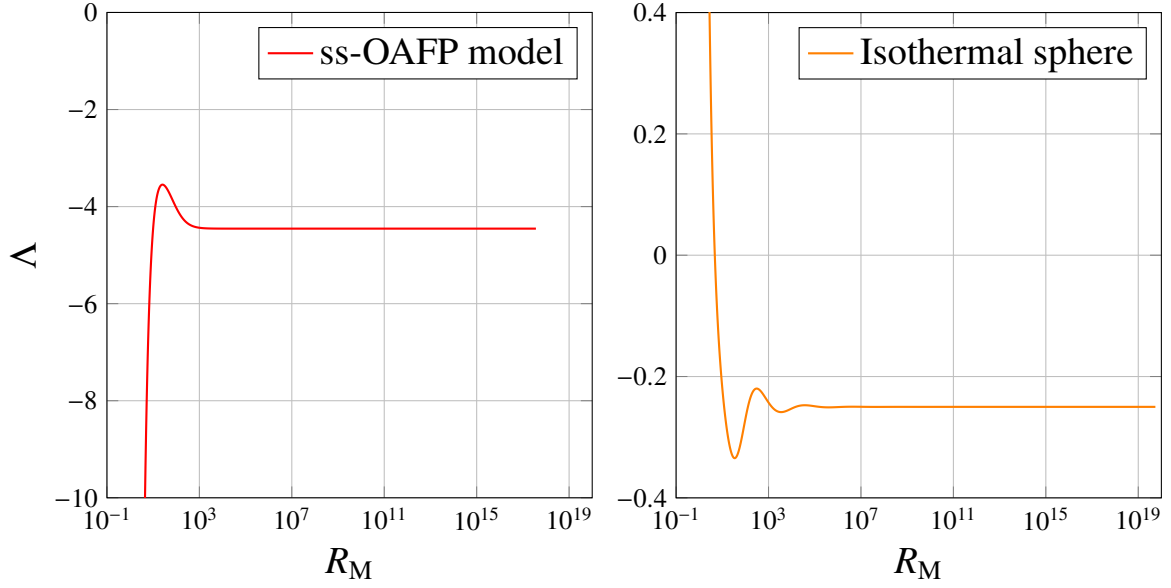


Figure 6: Dimensionless normalized total energies for the ss-OAFP model and isothermal sphere. As  $R_M \rightarrow 0$  the energies monotonically decreases for the former and increases for the latter. The curve for the isothermal sphere was obtained using the numerical code in (Ito et al., 2018).

kinetic-, local- and thermodynamic- temperatures to dimensionless forms

$$\eta^{(\text{kin})} = \frac{GM(R_M r_t(t_c), t_c)}{k_B T^{(\text{kin})}(R_M r_t(t_c))} = \frac{M}{T^{(\text{kin})} R_M}, \quad (3.3a)$$

$$\eta^{(\text{loc})} = \frac{GM(R_M r_t(t_c), t_c)}{k_B T^{(\text{loc})}(R_M r_t(t_c))} = \frac{M}{T^{(\text{loc})} R_M}, \quad (3.3b)$$

$$\eta^{(\text{con})} = \frac{\beta^{(\text{con})} R_M r_t(t_c)}{GM(R_M r_t(t_c))^2} = -\frac{S(\Phi_M)}{R_M}. \quad (3.3c)$$

Figure 7 depicts the dimensionless inverse temperatures  $\eta^{(\text{kin})}$ ,  $\eta^{(\text{loc})}$  and  $\eta^{(\text{con})}$  of the ss-OAFP model, compared to the corresponding temperature  $\eta$  of the isothermal sphere. All the temperatures monotonically decreases as  $R_M$  increases until they reach their minimum values. Only  $\eta^{(\text{con})}$  diverges at large  $R_M$ , which implies that the inverse temperature  $\beta^{(\text{con})}$  is not correctly regularized. Since the ss-OAFP model behaves like a polytropic sphere of  $m = \beta_o + 3/2$  at large  $R_M$ , one must regularize  $\beta^{(\text{con})}$  using the regularization made in (Taruya and Sakagami, 2002; Chavanis, 2002b).

### 3.2. Caloric curve

A caloric curve provides the characteristics of heat capacity of the ss-OAFP model. Dimensionless energy (3.1) and temperatures (3.3) construct caloric curves at constant volume (Figure 8). Based on Legendre transform, the graphs relate to the heat capacity  $C_V$ . For example, the kinetic temperature relates to  $C_V$  as follows

$$\left( \frac{\partial \frac{1}{\Lambda}}{\partial \eta^{(\text{kin})}} \right)_{R,M} = \left( \frac{\partial \frac{1}{\Lambda}}{\partial \eta^{(\text{kin})}} \right)_{V, N_{\text{tot}}} = \frac{C_V [T^{(\text{kin})}]^2}{M E_{\text{tot}}^2}. \quad (3.4)$$

Hence, the slope of the tangent to the caloric curve shows the sign of the heat capacity. The advantage of the caloric curve approach is to provide a simple topological understanding for the (linear) stability of systems in statistical (e.g. micro-canonical- and canonical-) ensembles without solving the corresponding eigenvalue problem (Katz, 1978, 1979, 1980). Since the ss-OAFP model does not achieve an equilibrium system, the rest discusses the heat capacity of the ss-OAFP model and its singularity to analogically understand the thermodynamical aspects, compared to the corresponding caloric curve for the isothermal sphere.

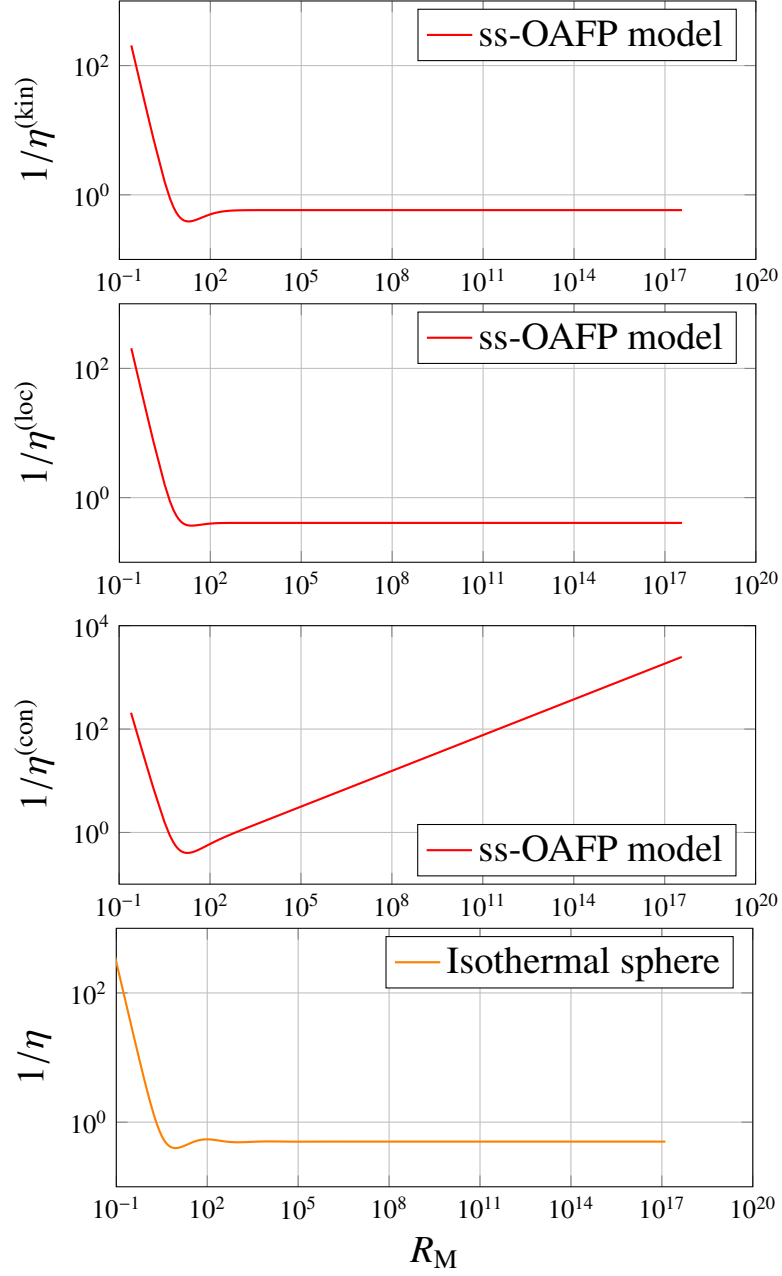


Figure 7: Dimensionless temperatures of the ss-OAFP model and temperature  $1/\eta$  isothermal sphere. The curve for the latter was obtained using the numerical code in (Ito et al., 2018)

### 3.2.1. Singularities in caloric curve of the ss-OAFP model

The heat capacity of the ss-OAFP model has singularities at small radii, which differs from the case of the isothermal sphere. Figure 8 depicts the caloric curves for the normalized energy  $\Lambda$  against the normalized inverse temperatures  $\eta^{(\text{kin})}$ ,  $\eta^{(\text{con})}$  and  $\eta^{(\text{loc})}$ . All the caloric curves show negative heat capacity at small radii while they have different characteristics at larger radii after passing through their turning points. The turning points of the caloric curves (Table 2) occur very close to each other in radius ( $R \approx 18 \sim 24$  for  $C_V \rightarrow \infty$  and  $R \approx 25$  for  $C_V = 0$ ). Perhaps, this is consistent with the nature of gravothermal instability. The negative heat capacity of the core originates from the core being nearly self-gravitating, independent of the halo or being in micro-canonical ensemble (D. Lynden-Bell and Royal, 1968; Thirring, 1970; Lynden-Bell and Lynden-Bell, 1977)<sup>7</sup>. This implies that regardless of kinds of walls (adiabatic or thermal) and ensemble (micro-canonical or canonical), the wall less affects any dynamics of the core. Hence, the singular behaviors in the heat capacity could occur very close to each other in radius *beyond* the radii  $R = 4.31$  and  $R = 3.31$  at which the heat- and stellar fluxes reach their maximum. This property is the distinct difference from the isothermal sphere. In case of the isothermal sphere, the radii at which the singularities occur are relatively away from each other at small radii ( $R = 34.9$  for  $C_V \rightarrow \infty$  and  $R = 8.9$  for  $C_V = 0$ ).

---

<sup>7</sup>For an isolated self-gravitating system, the Virial theorem states  $2KE + PE = 0$ , so  $E_{\text{tot}} = -KE$  (e.g. Heggie and Stevenson, 1988; Binney and Tremaine, 2011). Hence, the kinetic heat capacity is  $C_V \propto E_{\text{tot}}/KE < 0$ . As Thirring (1970) originally pointed out, the energy range of a system with negative heat capacity in micro-canonical ensemble corresponds to that with phase transition in canonical ensemble. Simply, canonical ensemble applies to the isothermal sphere at radii smaller than  $R = 8.9$  and micro-canonical ensemble at radii smaller than  $R = 34.9$  (See Table 2 for the value of radii.). The heat capacity is positive on  $0 < R < 8.9$  and negative on  $8.9 < R < 34.9$ .

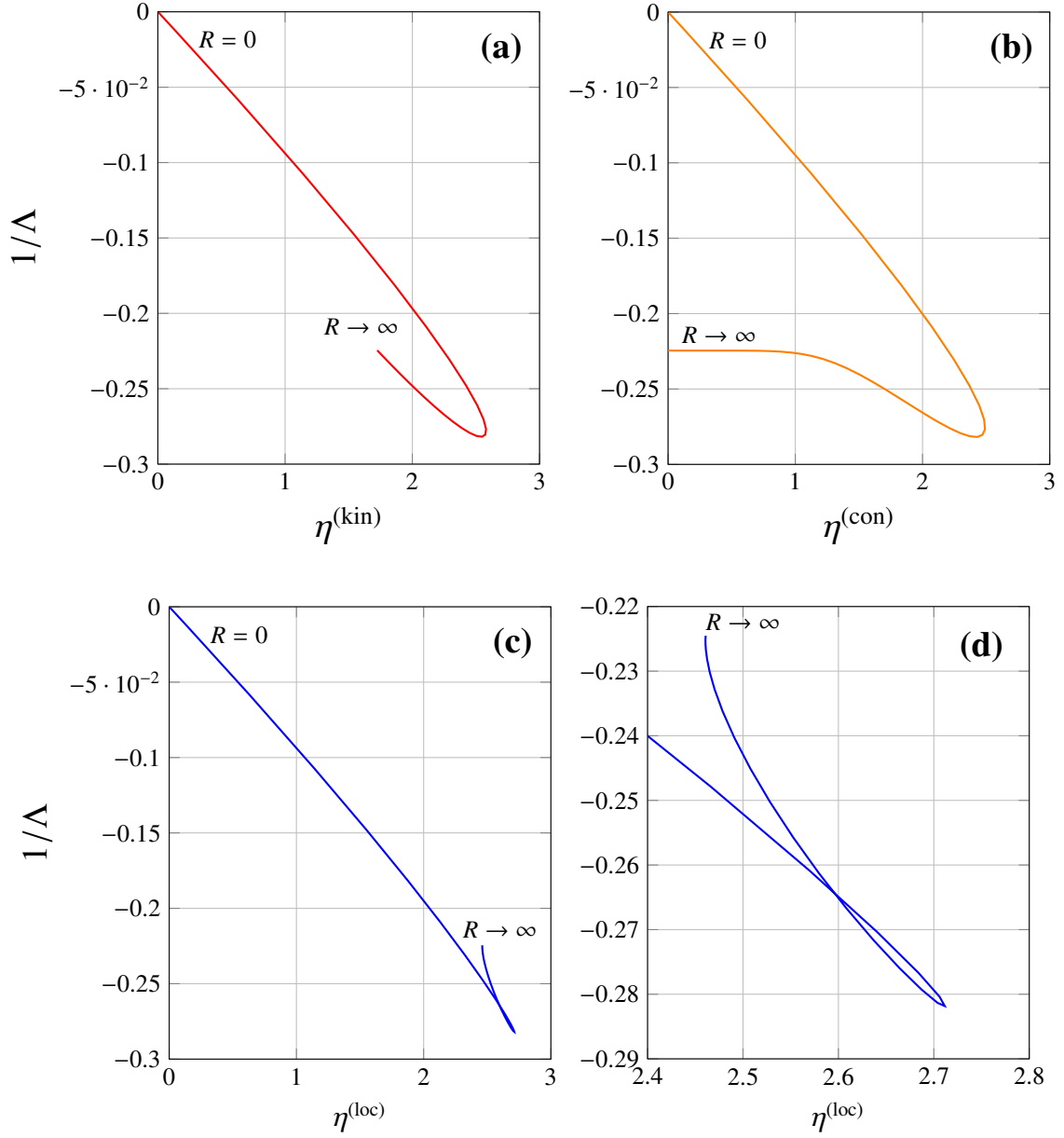


Figure 8: Caloric curves for the dimensionless- total energy  $\Lambda$  and temperatures **(a)**  $\eta^{(\text{kin})}$ , **(b)**  $\eta^{(\text{con})}$  and **(c)**  $\eta^{(\text{loc})}$ . **(d)** Magnification of **(c)** around the turning points. All the curves start at  $(0, 0)$  that corresponds to  $R = 0$ . For graphing, the ordinates are a reciprocal of  $\Lambda$ , hence the tangents to the curves represent the sign of  $C_V$ .

#### 4. Cause of negative heat capacity

Since the ss-OAFP model is at a non-equilibrium state, the self-gravity of the model does not cause negative heat capacity unlike (nearly) isolated self-gravitating systems at a state of equilibrium. The present section details possible cause of the negativeness especially focusing on the core of the model, accordingly only the kinetic heat capacity is discussed for simplicity. First, Section 4.1 introduces a simple analytical method to discuss the heat capacity based on Virial and total energy. This method shows that the shallow potential well at the center of the isothermal sphere causes positive kinetic heat capacity. On one hand, it also shows that the negative heat capacity

	$C_V \rightarrow \infty$				$C_V = 0$			
	$\eta$	$\Lambda$	$R_M$	$D(0)/D(R_M)$	$\eta$	$\Lambda$	$R_M$	$D(0)/D(R_M)$
Kinetic	2.580	-3.599	19.2	36.6	2.540	-3.548	25.4	74.85
Local	2.712	-3.549	24.1	65.8	2.711	-3.548	25.4	74.85
Thermodynamic	2.492	-3.633	17.9	30.3	2.418	-3.548	25.4	74.85
IS		-0.335	34.4	709	2.52		8.99	32.1

Table 2: First turning points of caloric curves at small radii. The Data for IS are the corresponding values for the isothermal sphere (e.g. Antonov, 1962; D. Lynden-Bell and Royal, 1968; Padmanabhan, 1989; Chavanis, 2002a).

originates from the deep potential well (or large scaled escape energy) at the center of the core in the ss-OAFP model. Lastly, Section 4.2 shows that the high temperature and collisionless limit of the core may cause the negative heat capacity by comparing the present work to existing works.

#### 4.1. Virial and total energy to discuss heat capacity at the center of the core

The heat capacity at the center of the ss-OAFP model can be discussed by the Virial and total energy  $E_{\text{tot}}$  (equation (2.8d))

$$\mathcal{V} \equiv -2\text{KE} - \text{PE} = - \int_0^{R_M} dR \int_{\Phi}^0 dE \Omega_{\text{mic}}(E, \Phi) R^2(E) (E - \Phi)^{3/2}, \quad (4.1a)$$

$$E_{\text{tot}} = \int_0^{R_M} dR \int_{\Phi}^0 dE \Omega_{\text{can}}(E, \Phi) R^2(E) (E - \Phi)^{3/2}, \quad (4.1b)$$

where

$$\Omega_{\text{mic}}(E, \Phi) = 2F(E) + \frac{\Phi}{3} \frac{dF}{dE}, \quad (4.2a)$$

$$\Omega_{\text{can}}(E, \Phi) = F(E) + \frac{\Phi}{3} \frac{dF}{dE}. \quad (4.2b)$$

Equations (4.2a) and (4.2b) present a simple analytical method to determine the sign of heat capacity in the core. Since the present focus is the center of the cores of star clusters, one may assume stars follow Maxwellian DF with escape energy  $\chi_{\text{esc}}$ ; the dimensionless DF reads  $F(E) = \exp[\chi_{\text{esc}} E]$ . Then,  $\Omega_{\text{mic}}$  and  $\Omega_{\text{con}}$  reduce to

$$\Omega_{\text{mic}}(E, \Phi) = e^{\chi_{\text{esc}} E} \left( 2 + \frac{\chi_{\text{esc}}}{3} \Phi \right), \quad (4.3a)$$

$$\Omega_{\text{con}}(E, \Phi) = e^{\chi_{\text{esc}} E} \left( 1 + \frac{\chi_{\text{esc}}}{3} \Phi \right). \quad (4.3b)$$

Change in the sign of heat capacity depends on

$$\Phi^{(\text{mic})} = -\frac{6}{\chi_{\text{esc}}}, \quad (4.4a)$$

$$\Phi^{(\text{can})} = -\frac{3}{\chi_{\text{esc}}}. \quad (4.4b)$$

These equations may be also related to the singularities in heat capacity.<sup>8</sup>

<sup>8</sup>Equation (4.4a) corresponds to the Virial being zero, that is, the thermal pressure at the adiabatic wall is zero. This determines the upper limit radius. Beyond the radius, micro-canonical ensemble can not apply to a self-gravitating system if the system is at a state of equilibrium. Equation (4.4b) corresponds to  $E_{\text{tot}}$  being zero, that is,  $E_{\text{tot}}$  is dominated by PE. This is a minimum condition that an equilibrium self-gravitating system does not exist in canonical ensemble. Under proper thermodynamic limit, the dimensionless total energy  $\Lambda$  reaches an extremum (singular point) as  $R_M$  increases since, as large  $R_M$ ,  $E_{\text{tot}}$  is proportional to  $M^2 G / R_M$ . At radii larger or smaller than the singular point, the sign of  $C_V$  possibly changes.

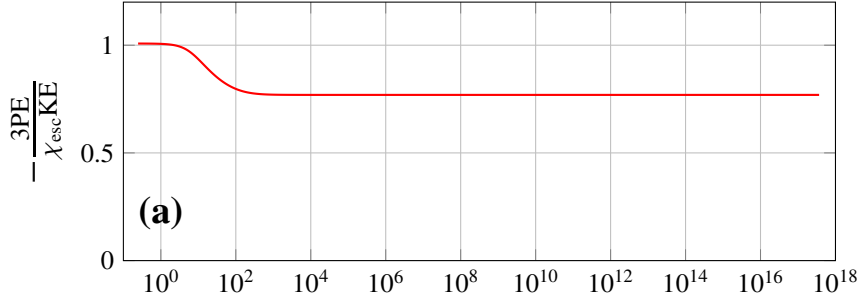


Figure 9: Ratio of -PE/KE to  $\chi_{\text{esc}}/3$

The present section relies on the approximation  $F = e^{\chi_{\text{esc}} E}$ , hence one needs to test the approximation. Figure 9 shows the ratio  $-\text{PE}/\text{KE}$  regularized by  $3/\chi_{\text{esc}}$ , which is a direct graphical representation for Equation 4.2a. The value reaches unity at  $R \approx 0$ , which validates the approximation of the DF to  $e^{\chi_{\text{esc}} E}$  at the center of the core.

The rest applies equations (4.3a) and (4.3b) to the kinetic heat capacities of isothermal sphere (Section 4.1.1) and (ii) of the ss-OAFP model (Section 4.1.2).

#### 4.1.1. Positive kinetic heat capacity at the center of the isothermal sphere

First the isothermal sphere ( $\chi_{\text{esc}} = 1$ ) is discussed whose kinetic heat capacity is positive at the center of the core due to the shallow potential well. The relation between the potential well and  $R_M$  is known (see e.g. D. Lynden-Bell and Royal, 1968; Padmanabhan, 1989). As  $R_M \rightarrow \infty$  the potential well deepens like  $\beta\phi(0) = -2 \ln[R] - 2$  due to the relationship  $\beta\phi(0) = -\Phi(R_M) - M/R_M$ . Hence, as  $R_M \rightarrow \infty$  the potential well gets deeper and the total energy decreases. On one hand, for small  $R_M$  such as  $R_M \ll 1$ ,  $\beta\phi(0) = -R_M^2/6 - 1$ . Hence, even if  $R_M = 1$ ,  $E_{\text{tot}}$  and  $\mathcal{V}$  are necessary positive.  $E_{\text{tot}}$  increases monotonically with  $R_M$  (due to the integrand being positive). Also, the kinetic energy monotonically increases with  $R_M$  at all radii (since local kinetic energy is always positive). KE and  $E_{\text{tot}}$  are zero at  $R_M = 0$  and are made in dimensionless form by the same factor (Section 3). As a result, the kinetic heat capacity is positive in the core for the isothermal sphere due to the shallow potential well. This is the case that one may consider the core of the isothermal sphere an ‘ordinary’ ideal gas (since the m.f. potential less affects the state of core).

#### 4.1.2. Negative heat capacity at the center of the ss-OAFP model

In case of the ss-OAFP model, the negative kinetic heat capacity at the center of the core is caused by the deep potential well. One still can use equations (4.2a) and (4.2b) with  $\chi_{\text{esc}} = 13.88$ . This is since the reference DF  $F_o(E)$  well fits the exponential of  $\chi_{\text{esc}} E$  on  $-1 < E \lesssim -0.5$  and  $\exp[-\chi_{\text{esc}} 0.5]$  contributes to the integrals (equations (4.1a) and (4.1b)) only by a small fraction ( $\sim 1 \times 10^{-3}$ ). Also, thanks to the self-similarity of the ss-OAFP model, the potential  $\Phi$  at  $R_M \approx 0$  is not related to the wall radius  $R_M$  unlike the isothermal sphere. Hence, one can discuss the heat capacity based only on local property of the ss-OAFP model. The known approximation,  $\Phi(R_M \approx 0) = -1 + R^2/6$ , infers that  $E_{\text{tot}}$  and  $\mathcal{V}$  are negative at  $R_M < 2.17$  and  $R_M < 1.85$ . Accordingly,  $E_{\text{tot}}$  decreases with  $R_M$  at small radii (due to the integrand being negative). Also, the kinetic energy increases at all radii as  $R_M$  increases. Hence, the ss-OAFP model must have a negative heat capacity at small radii ( $R_M \lesssim 2.2$ ) in the core. One may recall  $\Phi(R = 0)$  is set to  $-1$  for numerical integration of the ss-OAFP system. Yet, through equations (4.2a) and (4.2b), a large  $\chi_{\text{esc}}$  is equivalent to a deep potential well. Hence, the negative heat capacity is the consequence of the deep potential well. This is the case that the present work considered the ss-OAFP model behaves as an ‘exotic’ ideal gas.

#### 4.2. The cause of negative heat capacity compared to the previous works

The present section compares the negative heat capacity of the core of the ss-OAFP model to that of a simple model (Section 4.2.1) and more realistic model to discuss the cause of the negativity (Section 4.2.2).

#### 4.2.1. A simple understanding of the negative heat capacity in the core of the ss-OAFP model

In case of the ss-OAFP model, small number of stars are left in the deep potential well due to the high escape energy (Figure 5) while the spatial profile of stars in the halo (or the halo density) is time-independent.<sup>9</sup> Hence, majority of the stars in the core stays in the potential well produced through heat- and-particle fluxes. The stars tightly bounds each other every time they lose particle- and kinetic- energy through the fluxes due to the conservation of energy<sup>10</sup>. This means if one enclose the stars in the core by an adiabatic wall of small  $R_M$  they may behave like particles interacting via short-range pair potential (Posch et al., 1990; Posch and Thirring, 2005; Thirring et al., 2003) though, this is not the case. For such systems, the majority of energy band (level) are available to particles meaning the particles can be well mixed and the negative heat capacity occurs to only limited energy band that corresponds to a phase transition. On one hand, the present work deals with only the collapsed-state. Also, the energy band that shows negative specific heat is broad in sense it covers at least the energy that are available to particles in the potential well (or in the core with  $R_M = 1$ ). This situation is alike the characteristics of the negative specific heat reported for collisionless particles in potential well (Thirring et al., 2003; Carignano and Gladich, 2010).

For the core of the ss-OAFP model being enclosed by an adiabatic wall, the initial conditions are not important since the core is a well-relaxed non-equilibrium state. The two key points here are that the temperature at the center is high (Figure 7) and that the probability to find stars in the core is low in the core. For the latter, the total number  $N_M(\equiv M/m)$  of stars in the core is a small fraction e.g.  $N_M \approx 5.6 \times 10^{-3}$  at  $R_M = 1$  and  $N_M \approx 1$  at radius the flattening in  $\Phi$  ceases (Figure 10 (a)). Hence, a proper zeroth-order approximation is collisionless limit. In this limit, the core behaves like a collisionless ideal gas as typically assumed for the isothermal sphere (e.g. Katz, 1978). This means the stars behave as if they were non-interacting particles traveling only under the effect of m.f. potential  $\Phi$ . Figure 10 (b) shows the potential well  $\Phi(R_M)$  and mean total energy per unit mass  $E_{\text{tot}}/M$ . The stars in the core can stay in the deep potential well to develop the core-collapse, however due to the high temperature (kinetic energy) some of stars need to spill out of the potential well. The corresponding process is that one may imagine to expand the adiabatic wall. Then from the figure, the total kinetic energy per unit mass obviously decreases while the total energy increases with radius. Hence, the negative heat capacity is the outcome of the deep potential well together with the high temperature and low total number of stars in the core. This graphical method (Thirring et al., 2003; Carignano and Gladich, 2010) would be the simplest way to understand the negative heat capacity in the present case.

#### 4.2.2. Comparison to an existing realistic model

Lastly, the rest compares the core of the ss-OAFP model to the  $N$ -body simulations (Komatsu et al., 2010, 2012) executed under the physical condition similar to the core. Strictly speaking, systems similar to the ss-OAFP model does not only exist in nature but also as a result of numerical  $N$ -body simulation<sup>11</sup> since complete core-collapse itself is a mathematical concept. Yet, some features of complete core-collapse should appear at the early stage of core collapse as shown in (Cohn, 1980). The basic condition that one must consider is that a self-gravitating system of small  $N$  particles must be enclosed by a wall undergoing a core-collapse but losing kinetic-energy and stars outside the wall due to heat- and particle- fluxes. Also, the system must be large enough to form core-halo structure to make the fluxes occur. (Komatsu et al., 2010, 2012) embodies such conditions by using a  $N$ -body simulation for  $N = 125 \sim 250$ . To achieve the condition, they used a partially permeable wall through which the evaporation (escape) rate of particles from the system can change by controlling the escape energy, that is, the degree of permeability.

The results of (Komatsu et al., 2010, 2012) well reflect the core-collapsing core-inner halo structure. In (Komatsu et al., 2012) they obtained a Maxwellian-like velocity distribution function, and showed not only negative specific but also

<sup>9</sup>As  $R_M \gg 1$ , the halo density  $\rho(r, t)$  is independent of the dynamics in the core or relaxation evolution in self-similar analysis, which provides  $d\rho(r, t)/dt = 0$ , hence  $D(R) \propto R^{-\alpha}$  and  $\rho_t \propto r_t^{-\alpha}$ .

<sup>10</sup>One may recall the failure of the Bohr model in which electron releases electromagnetic radiation due to the acceleration and deeply penetrates into the potential well around the ion. In a similar way, for stellar encounter, stars can approach each other even on scales of stellar size. Or recall the 'fly-by' effect when a satellite in space needs an extra energy. It must first lose kinetic energy (through a friction from gases) near an astrophysical object and then it can orbit in deep potential well of the object. Finally, the satellite can obtain a kinetic energy from the potential.

<sup>11</sup>The former is explained in (Ito, 2020) (and our third paper of the present work) while the latter is because it is not easy to achieve the 'complete' core collapse like the ss-OAFP model other than using continuum models. Not only the effect of binary stars stops core collapse but also large  $N \approx 10^5$  costs unfeasible CPU to achieve the complete collapse. Hence, one needs to find a similarity of the ss-OAFP model to self-gravitating system of less  $N$  stars.



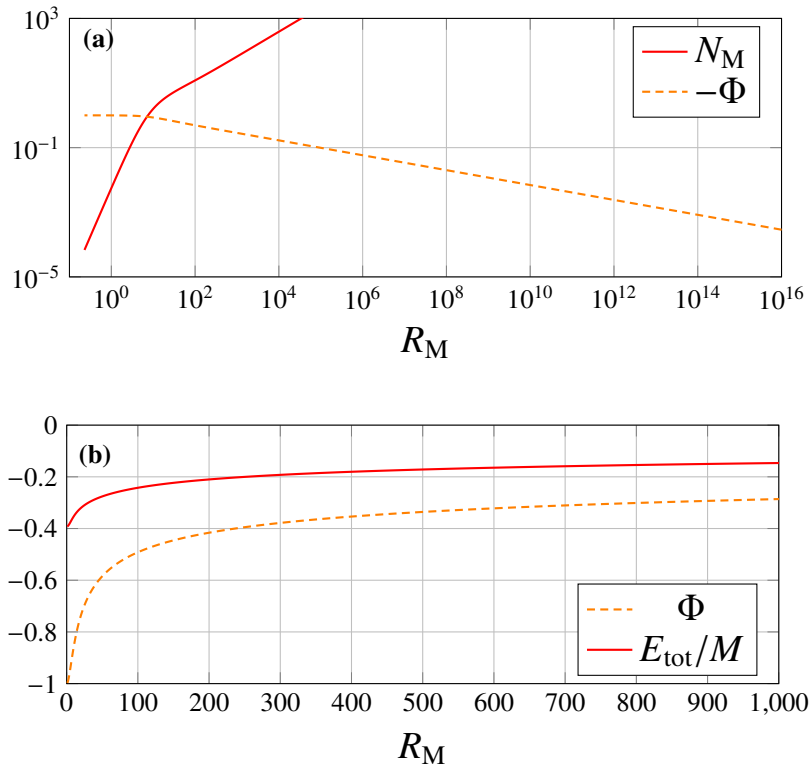


Figure 10: Dimensionless m.f. potential  $\Phi$  and **(a)** total number of stars for the ss-OAFP model enclosed by an adiabatic wall at  $R_M$  and **(b)** normalized mean energy per unit mass of the ss-OAFP model.

greater velocity gradient with increasing time (like Cohn, 1980), together with density and dispersion well correlating like Figure 1(a). On one hand, in (Komatsu et al., 2010) they used stellar polytropes to characterize the non-equilibrium state of their model using the same method. They found the polytrope of  $m \sim 9$  is initially close to their model with a negative value of  $\Lambda$  but it begins to deviate from the model with decreasing  $\Lambda$  as the collapse proceeds. They insisted the deviation occurred because the kinetic temperature is not suitable to describe the non-equilibrium state. Yet, it would less matter. Smaller  $\Lambda$  means the the core size is relatively large and close the wall radius. This corresponds to, in the present model, radius  $R_M$  approaches the center of the core where the kinetic temperature can be reasonably defined due to the relaxation. The reason the deviation occur would be because the polytrope itself is not proper to describe the system with negative heat capacity. The caloric curve for the polytropes of  $m > 5$  spirals as  $\Lambda$  decreases, showing marginal instabilities (or successive instability with increasing radius) (Chavanis, 2002b, 2003). This corresponds with collapsed state with large  $R_M$  which does not exist due to the instability. On one hand, the caloric curve for the ss-OAFP model provides only negative heat capacity at small  $\Lambda$  (or monotonically increasing  $1/\eta^{(kin)}$  with decreasing  $\Lambda$ ). This well matches the qualitative nature of the curve reported in (Figure 5 in Komatsu et al., 2010).

## 5. Conclusion

In the present paper we aimed at showing the basic physical features of the ss-OAFP model focusing on the core of the model and negative heat capacity. We first discussed the local and global properties of the ss-OAFP model. The model shows similar properties compared to the self-similar conductive model though, we found the equation of state in the core is local ideal gas  $p = 1.0\rho/\chi_{\text{esc}}$  while it is polytropic  $p = 0.5\rho^\Gamma/\chi_{\text{esc}}$  at large radii. Since the the center of the core can be described by the state of the polytropic index  $m = 177$ , it shows the incompleteness of Maxwellian DF even at the center. We also showed negative heat capacity at constant volume of the model by constructing regularized quantities. A unique feature of the ss-OAFP model originates from it being a nonequilibrium system. While the core is well-relaxed state, it can achieve negative heat capacity since stars in the core can behave like collisionless particles due to high temperature and low total number of stars in its deep potential. This cause is different from equilibrium self-gravitating systems such as isothermal sphere for which negative heat capacity occurs as a result of phase transition or when the system is large enough to be isolated from the ambient stars/gas in sense that the Virial reaches zero. The Virial of the ss-OAFP model is not zero, rather positive. Also, the ss-OAFP model is not related to the cases in which equilibrium systems can show negative heat capacity because of the initial conditions. The present analysis reemphasizes that the negative heat capacity can be peculiar to self-gravitating non-equilibrium systems in addition to inhomogeneous equilibrium systems.

## Appendix A Regularization of total energy

The present Appendix explains the relationship between the regularization of  $E_{\text{tot}}$  and Poisson equation for the ss-OAFP model. A proper integral of Poisson equation in inverse form (Ito, 2020) with respect to  $R$  reads

$$R^2 \frac{d\Phi}{dR} = M, \quad (\text{A.1})$$

Since the ss-OAFP model has power law boundary condition  $\Phi \propto R^{-\alpha}$  at  $R \rightarrow \infty$ , one can employ the identity  $\frac{d\Phi}{dR} = -\alpha\Phi/R$ . Accordingly, the Poisson equation at large  $R$  reduces to

$$\Phi = -\frac{M}{R\alpha}. \quad (\text{A.2})$$

The total energy  $E_{\text{tot}}$  at  $R \rightarrow \infty$  is obviously proportional to  $M$ . The domain of  $E_{\text{tot}}$  is  $(\Phi, 0)$ . Hence, proper change of variable makes the factor  $(E - \Phi)$  be proportional to  $\Phi$ . As a result,

$$E_{\text{tot}} \propto \frac{M^2}{R}. \quad (\text{A.3})$$

Although one may choose different quantities to regularize  $E_{\text{tot}}$ , we focus on heat capacity at constant volume. This means total number  $N$  and volume  $V$  are constant, that is, total mass  $M$  and radius  $R$  are constant (under Legendre transformation). Hence, regularizing  $E_{\text{tot}}$  originates from the characteristics of the Poisson equation.

## Acknowledgements

The present work is partial fulfillment of the degree of Philosophy at CUNY graduate center.

- Aguado, A., Jarrold, M. F., may 2011. Melting and freezing of metal clusters. *Annual Review of Physical Chemistry* 62 (1), 151–172.  
URL <https://doi.org/10.1146%2Fannurev-physchem-032210-103454>
- Antonov, V., 1962. Most probable phase distribution in spherical star systems and conditions for its existence. *Vest. Leningrad Univ.* 7, 135.
- Binney, J., Tremaine, S., 2011. *Galactic Dynamics*. Princeton university press.
- Borderie, B., Frankland, J., mar 2019. Liquid–gas phase transition in nuclei. *Progress in Particle and Nuclear Physics* 105, 82–138.  
URL <https://doi.org/10.1016%2Fj.ppnp.2018.12.002>
- Brilliantov, N. V., Formella, A., Pöschel, T., feb 2018. Increasing temperature of cooling granular gases. *Nature Communications* 9 (1).  
URL <https://doi.org/10.1038%2F41467-017-02803-7>
- Carignano, M. A., Gladich, I., jun 2010. Negative heat capacity of small systems in the microcanonical ensemble. *EPL (Europhysics Letters)* 90 (6), 63001.  
URL <https://doi.org/10.1209%2F0295-5075%2F90%2F63001>
- Chavanis, P. H., jan 2002a. Gravitational instability of finite isothermal spheres. *Astronomy & Astrophysics* 381 (1), 340–356.  
URL <https://doi.org/10.1051%2F0004-6361%3A20011438>
- Chavanis, P. H., may 2002b. Gravitational instability of polytropic spheres and generalized thermodynamics. *Astronomy & Astrophysics* 386 (2), 732–742.  
URL <https://doi.org/10.1051%2F0004-6361%3A20020306>
- Chavanis, P. H., mar 2003. Gravitational instability of isothermal and polytropic spheres. *Astronomy & Astrophysics* 401 (1), 15–42.  
URL <https://doi.org/10.1051%2F0004-6361%3A20021779>
- Claydon, I., Gieles, M., Varri, A. L., Hoggie, D. C., Zocchi, A., may 2019. Spherical models of star clusters with potential escapers. *Monthly Notices of the Royal Astronomical Society* 487 (1), 147–160.  
URL <https://doi.org/10.1093%2Fmnras%2Fstz1109>
- Cohn, H., dec 1980. Late core collapse in star clusters and the gravothermal instability. *The Astrophysical Journal* 242, 765.  
URL <https://doi.org/10.1086%2F158511>
- D. Lynden-Bell, R. W., Royal, A., feb 1968. The gravo-thermal catastrophe in isothermal spheres and the onset of red-giant structure for stellar systems. *Monthly Notices of the Royal Astronomical Society* 138 (4), 495–525.  
URL <http://dx.doi.org/10.1093/mnras/138.4.495>
- de Vega, H., Sánchez, N., mar 2002. Statistical mechanics of the self-gravitating gas: I. thermodynamic limit and phase diagrams. *Nuclear Physics B* 625 (3), 409–459.  
URL <https://doi.org/10.1016%2Fs0550-3213%2802%2900025-1>
- DéAgostino, M., Botvina, A., Bruno, M., Bonasera, A., Bondorf, J., Bougault, R., Désesquelles, P., Geraci, E., Gulminelli, F., Iori, I., Neindre, N. L., Margagliotti, G., Mishustin, I., Moroni, A., Pagano, A., Vannini, G., apr 1999. Thermodynamical features of multifragmentation in peripheral  $^{136}\text{Xe} + ^{136}\text{Xe}$  collisions at 35 a MeV. *Nuclear Physics A* 650 (3), 329–357.  
URL <https://doi.org/10.1016%2Fs0375-9474%2899%2900097-4>
- DéAgostino, M., Gulminelli, F., Chomaz, P., Bruno, M., Cannata, F., Bougault, R., Gramegna, F., Iori, I., Neindre, N. L., Margagliotti, G., Moroni, A., Vannini, G., feb 2000. Negative heat capacity in the critical region of nuclear fragmentation: an experimental evidence of the liquid-gas phase transition. *Physics Letters B* 473 (3–4), 219–225.  
URL <https://doi.org/10.1016%2Fs0370-2693%2899%2901486-0>
- Destri, C., de Vega, H., feb 2007. Dilute and collapsed phases of the self-gravitating gas. *Nuclear Physics B* 763 (3), 309–329.  
URL <https://doi.org/10.1016%2Fj.nuclphysb.2006.10.028>
- Einarsson, B., nov 2004. Conditions for negative specific heat in systems of attracting classical particles. *Physics Letters A* 332 (5–6), 335–344.  
URL <https://doi.org/10.1016%2Fj.physleta.2004.09.066>
- Gobet, F., Farizon, B., Farizon, M., Gaillard, M. J., Buchet, J. P., Carré, M., Scheier, P., Märk, T. D., oct 2002. Direct experimental evidence for a negative heat capacity in the liquid-to-gas phase transition in hydrogen cluster ions: Backbending of the caloric curve. *Physical Review Letters* 89 (18).  
URL <https://doi.org/10.1103%2Fphysrevlett.89.183403>
- Hoggie, D. C., Stevenson, D., jan 1988. Two homological models for the evolution of star clusters. *Monthly Notices of the Royal Astronomical Society* 230 (2), 223–241.  
URL <http://dx.doi.org/10.1093/mnras/230.2.223>
- Ingel, L. K., nov 2000. “negative heat capacity” of stratified fluids. *Journal of Experimental and Theoretical Physics Letters* 72 (10), 527–529.  
URL <https://doi.org/10.1134%2F1.1343157>
- Ito, Y., 2020. Self-similar orbit-averaged fokker-planck equation for isotropic spherical dense clusters (i) accurate pre-collapse solution.
- Ito, Y., Poje, A., Lancellotti, C., jan 2018. Very-large-scale spectral solutions for spherical polytropes of index  $m \lesssim 5$  and the isothermal sphere. *New Astronomy* 58, 15–28.  
URL <https://doi.org/10.1016%2Fj.newast.2017.07.003>
- Josephson, B. D., oct 1967. Inequality for the specific heat: I. derivation. *Proceedings of the Physical Society* 92 (2), 269–275.  
URL <https://doi.org/10.1088%2F0370-1328%2F92%2F2%2F301>
- Katz, J., aug 1978. On the number of unstable modes of an equilibrium. *Monthly Notices of the Royal Astronomical Society* 183 (4), 765–770.  
URL <https://doi.org/10.1093%2Fmnras%2F183.4.765>

- Katz, J., dec 1979. On the number of unstable modes of an equilibrium - II. Monthly Notices of the Royal Astronomical Society 189 (4), 817–822.  
URL <https://doi.org/10.1093/mnras/2F189.4.817>
- Katz, J., mar 1980. Stability limits for ‘isothermal’ cores in globular clusters. Monthly Notices of the Royal Astronomical Society 190 (3), 497–507.  
URL <https://doi.org/10.1093/mnras/2F190.3.497>
- Katz, J., Taff, L. G., Jan 1983. Stability limits for ‘isothermal’ cores in globular cluster models - Two-component systems. Apj 264, 476–484.
- Komatsu, N., Kiwata, T., Kimura, S., aug 2010. Thermodynamic properties of an evaporation process in self-gravitating N-body systems. Physical Review E 82 (2).  
URL <https://doi.org/10.1103/PhysRevE.82.021118>
- Komatsu, N., Kiwata, T., Kimura, S., feb 2012. Transition of velocity distributions in collapsing self-gravitating N-body systems. Physical Review E 85 (2).  
URL <https://doi.org/10.1103/PhysRevE.85.021132>
- Louis, P. D., Spurzem, R., 1991. Anisotropic gaseous models for the evolution of star clusters. Monthly Notices of the Royal Astronomical Society 251 (3), 408–426.  
URL <http://dx.doi.org/10.1093/mnras/251.3.408>
- Lynden-Bell, D., feb 1999. Negative specific heat in astronomy, physics and chemistry. Physica A: Statistical Mechanics and its Applications 263 (1-4), 293–304.  
URL [https://doi.org/10.1016/S0378-4371\(98\)00518-4](https://doi.org/10.1016/S0378-4371(98)00518-4)
- Lynden-Bell, D., Eggleton, P., jul 1980. On the consequences of the gravothermal catastrophe. Monthly Notices of the Royal Astronomical Society 191 (3), 483–498.  
URL <http://dx.doi.org/10.1093/mnras/191.3.483>
- Lynden-Bell, D., Lynden-Bell, R. M., dec 1977. On the negative specific heat paradox. Monthly Notices of the Royal Astronomical Society 181 (3), 405–419.  
URL <https://doi.org/10.1093/mnras/2F181.3.405>
- Lynden-Bell, D., Lynden-Bell, R. M., may 2008. Negative heat capacities do occur. comment on “critical analysis of negative heat capacities in nanoclusters” by Michaelian K. and Santamaría-Holek I. EPL (Europhysics Letters) 82 (4), 43001.  
URL <https://doi.org/10.1209/2F0295-5075/2F82/2F43001>
- Michaelian, K., Santamaría-Holek, I., jul 2007. Critical analysis of negative heat capacity in nanoclusters. Europhysics Letters (EPL) 79 (4), 43001.  
URL <https://doi.org/10.1209/2F0295-5075/2F79/2F43001>
- Michaelian, K., Santamaría-Holek, I., oct 2015. Dynamics and thermodynamics of nanoclusters. Entropy 17 (12), 7133–7148.  
URL <https://doi.org/10.3390/Entropy17107133>
- Michaelian, K., Santamaría-Holek, I., jun 2017. Invalid microstate densities for model systems lead to apparent violation of thermodynamic law. Entropy 19 (7), 314.  
URL <https://doi.org/10.3390/Entropy19070314>
- Michie, R. W., aug 1962. On the distribution of high energy stars in spherical stellar systems. Monthly Notices of the Royal Astronomical Society 125 (2), 127–139.  
URL <https://doi.org/10.1093/mnras/2F125.2.127>
- Padmanabhan, T., nov 1989. Antonov instability and gravothermal catastrophe - revisited. The Astrophysical Journal Supplement Series 71, 651.  
URL <https://doi.org/10.1086/2F191391>
- Posch, H. A., Narnhofer, H., Thirring, W., aug 1990. Dynamics of unstable systems. Physical Review A 42 (4), 1880–1890.  
URL <https://doi.org/10.1103/PhysRevA.42.1880>
- Posch, H. A., Thirring, W., dec 2005. Stellar stability by thermodynamic instability. Physical Review Letters 95 (25).  
URL <https://doi.org/10.1103/PhysRevLett.95.251101>
- Prabhu, N. V., Sharp, K. A., may 2006. Heat capacity in proteins. ChemInform 37 (19).  
URL <https://doi.org/10.1002/2Fchin.200619262>
- Schmidt, M., Kusche, R., Hippler, T., Donges, J., Kronmüller, W., von Issendorff, B., Haberland, H., feb 2001. Negative heat capacity for a cluster of 147 sodium atoms. Physical Review Letters 86 (7), 1191–1194.  
URL <https://doi.org/10.1103/PhysRevLett.86.1191>
- Spitzer, L. J., Shapiro, S. L., may 1972. Random gravitational encounters and the evolution of spherical systems. III. halo. The Astrophysical Journal 173, 529.  
URL <https://doi.org/10.1086/2F151442>
- Spitzer, L. S., jan 1988. Dynamical Evolution of Globular Clusters. Walter de Gruyter GmbH.  
URL <http://dx.doi.org/10.1515/9781400858736>
- Srivastava, B., aug 2001. Multifragmentation and the phase transition: A systematic study of the multifragmentation of 1a GeV au, 1a and kr. Pramana 57 (2-3), 301–313.  
URL <https://doi.org/10.1007/2Fs12043-001-0040-x>
- Takahashi, K., 1993. Self-similar solutions of the orbit-averaged fokker-planck equation: Application of the generalized variational principle. Publications of the Astronomical Society of Japan 45, 789–793.
- Taruya, A., Sakagami, M., apr 2002. Gravothermal catastrophe and Tsallis’ generalized entropy of self-gravitating systems. Physica A: Statistical Mechanics and its Applications 307 (1-2), 185–206.  
URL [http://dx.doi.org/10.1016/S0378-4371\(01\)00622-7](http://dx.doi.org/10.1016/S0378-4371(01)00622-7)
- Thirring, W., aug 1970. Systems with negative specific heat. Zeitschrift für Physik A Hadrons and nuclei 235 (4), 339–352.  
URL <https://doi.org/10.1007/2Fb01403177>
- Thirring, W., Narnhofer, H., Posch, H. A., sep 2003. Negative specific heat, the thermodynamic limit, and ergodicity. Physical Review Letters 91 (13).  
URL <https://doi.org/10.1103/PhysRevLett.91.130601>

Tsallis, C., 2009. Introduction to Nonextensive Statistical Mechanics. Springer Science + Business Media.  
URL <http://dx.doi.org/10.1007/978-0-387-85359-8>